Infrared imaging of thermal areas

Bridget Y. Lynne and Rubén Yagüe
Institute of Earth Science and Engineering, University of Auckland, 58 Symonds St, Auckland 1142, New Zealand. E-mail: b.lynne@auckland.ac.nz, r.yague@auckland.ac.nz

Abstract
Heat discharges at the surface by way of thermal features such as hot springs, fumaroles and steaming ground. An understanding of discharging heat is important for geothermal exploration, as it provides a guide to the geothermal power potential of the reservoir. One way to determine the amount of heat discharging in active thermal areas is to measure the temperature of the surface features. In three New Zealand geothermal fields, we measured temperatures of surface manifestations using: 1) a temperature probe, 2) an infrared thermometer and 3) an infrared camera. Using all three techniques we documented the temperatures in 12 alkali chloride hot springs and channels, six acid sulfate hot springs, six mud pools, nine areas of steaming ground and seven fumaroles. This enabled a direct comparison of the temperatures obtained using the different techniques for each feature type. Our study revealed that regardless of which measuring device was used, the temperatures measured in hot spring pools and channels showed minimal variation. In fumaroles and steaming ground areas, the correlation between temperature measuring devices was not as consistent. However, there was minimal temperature variation when we were within one meter of the steam features and when we altered the emissivity value to account for the higher reflectance due to the discharging steam. Our infrared camera enabled the quick identification of sites with increased temperature that were not easily accessible. It was also ideally suited for mapping the location of micro-fractures and vents that discharged heat and were not otherwise visible. Infrared imaging enables the mapping of subtle temperature differences establishing surface thermal gradients profiles. Alignment and orientation of areas discharging a higher-than-ambient temperature are also easily mapped. Infrared imaging contributes to our knowledge on the heat flow migration pathways, which contributes to the development of a conceptual model of a geothermal system.

Keywords: Superficial thermal manifestations, heat flow, infrared imaging, geothermal exploration.

Imágenes de infrarrojo en zonas termales

Resumen
El calor se descarga en superficie dando lugar a manifestaciones termales como manantiales termales, fumarolas y suelos vaporizantes. Es importante comprender la descarga de calor para la exploración geotérmica, ya que proporciona una pauta acerca de la energía geotérmica potencial del reservorio. Una forma de determinar la cantidad de calor que se descarga en áreas termales activas es midiendo la temperatura de las manifestaciones de superficie. En tres campos geotérmicos de Nueva Zelanda se midió la temperatura de manifestaciones superficiales utilizando: 1) un termómetro de cable, 2) un termómetro de infrarrojos y 3) una cámara de infrarrojos. Usando estas tres técnicas documentamos temperaturas en 12 manantiales termales y canales alcalinos clorurados, seis fuentes termales sulfatadas ácidas, seis albercas de lodo, nueve zonas de suelos vaporizantes y siete fumarolas. Esto nos permitió una comparación directa de las temperaturas obtenidas usando las distintas técnicas para cada tipo de manifestación. Nuestro estudio reveló que independientemente del dispositivo de medición, las temperaturas medidas en manantiales termales y canales mostraron una variación mínima. Pero en fumarolas y suelos vaporizantes la correlación entre los dispositivos de medición de temperaturas no fue tan consistente. Sin embargo, las variaciones de temperatura se volvían mínimas cuando estábamos

a menos de un metro de las manifestaciones de vapor y cuando modificamos el valor de la emisividad para contrarrestar la mayor reflectancia debido a la descarga de vapor. Nuestra cámara de infrarrojos nos permitió una rápida identificación de lugares con mayor temperatura, que no son fácilmente accesibles. También fue ideal para cartografiar la ubicación de micro-fracturas y conductos que descargaban calor y que no eran visibles de otra manera. Las imágenes de infrarrojo permiten cartografiar sutiles diferencias de temperatura y establecer perfiles de gradiente térmico en superficie. También permiten cartografiar fácilmente la alineación y orientación de áreas que descargan a una temperatura mayor que la ambiental. La captación de imágenes de infrarrojos contribuye al conocimiento de las vías de migración del flujo de calor, lo que contribuye al desarrollo de un modelo conceptual del sistema geotérmico.

Palabras clave: Manifestaciones termales superficiales, flujo de calor, imágenes de infrarrojo, exploración geotérmica.

1. Introduction

Geothermal exploration studies involve a step-wise approach whereby geological, geochemical and geophysical assessments of an area are undertaken to prove the existence of a resource at depth. One new method that can be introduced to the geologist's tool-kit at the initial stages of exploration is the use of an infrared camera. Imaging thermal manifestations and tracking heat flow gradient profiles at the surface is important when investigating an area for its geothermal potential. For our study we used an infrared camera, infrared thermometer and a temperature probe to measure the temperature of different thermal manifestations commonly found in geothermal settings.

There are few published reports on the use of a hand-held infrared camera for geothermal exploration but similar work has been done in volcanic settings in Mexico, where a hand-held infrared camera has been used to monitor the temperatures of fumaroles at Volcán de Colima, in Mexico (Stevenson and Varley, 2008). While this is a volcanic setting and not a geothermal environment, it is of interest as their work focussed on measuring fumarolic temperatures, a feature common to geothermal systems. Work done by Stevenson and Varley (2008) also reported their instruments were designed to operate at wavelengths with a low sensitivity to water vapour, which is the main discharge from the fumaroles. Therefore they modified their work to take measurements of the fumarole vent wall. Another report shows that as the measurement distance increases, so did the scattering of radiation along the path between the fumarole and the sensor. Therefore the closer you are to the feature, the more accurate the data (Ball and Pinkerton, 2006). According to other studies, the factors affecting temperature readings are: (1) poor focussing, (2) amount of cloud cover, (3) steam discharging from fumaroles, (4) viewing angle, and (5) the absorption of infrared by volcanic gases. (Stevenson and Varley, 2008; Oppenheimer et al., 2006). Thermal infrared (TIR) remote sensing data has been used to detect surface heat in geothermal areas in China (Qiming et al., 2011). TIR has been shown to be an effective technique for obtaining the land surface temperature. However, Qiming et al. (2011) document that data obtained using TIR techniques are affected by heat generated by solar radiation, topography and earthquakes. There are some reports of aerial infrared imaging of surface thermal features such as at Tauhara geothermal field, New Zealand, (Dickinson, 1975) and Kagoshima, Japan, (Yuhara, et al., 1978), but aerial infrared imaging is expensive and not commonly done for geothermal exploration. However, ASTER (Advanced Spaceborne Thermal Emission and Reflexion Radiometer) TIR (thermal infrared) is another technique that was successfully used for mapping temperature anomalies associated with geothermal activity at Bradys Hot Springs, Nevada, USA (Coolbaugh et al., 2006).

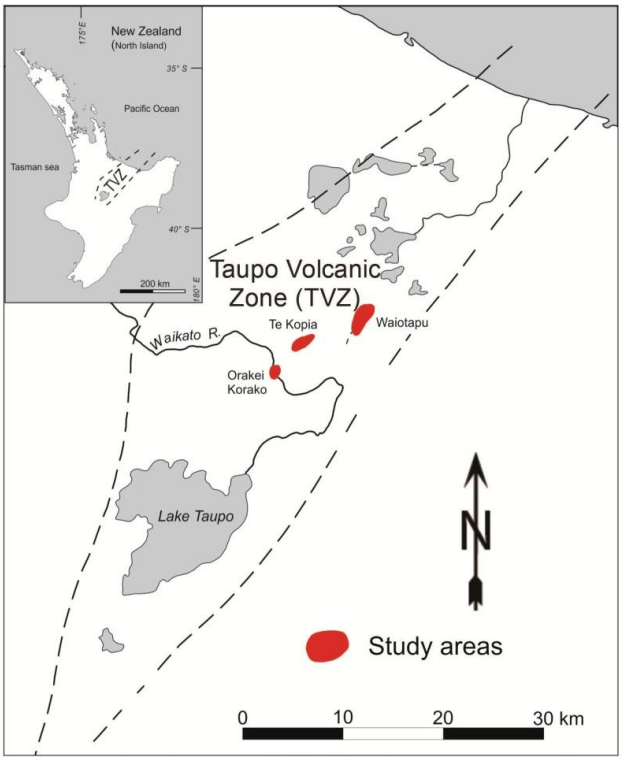

Fig. 1. Map of the Taupo Volcanic Zone (TVZ) showing the locations of Waiotapu, Te Kopia and Orakei Korako geothermal fields, our study sites. (In Table 1: location 1 = Waiotapu, location 2 = Te kopia, location 3 = Orakei Korako). Insert: Location of TVZ within the North Island of New Zealand.

Our study focuses on comparing temperature measurements of geothermal surface features using different techniques. We recorded temperature measurements of various types of thermal manifestations from three geothermal fields (Waiotapu, Orakei Korako and Te Kopia) all located within the Taupo Volcanic Zone, New Zealand (Fig. 1). From our data we could assess the suitability of each technique for the different types of thermal features. We also assessed the effect of emissivity on our recorded temperature measurements. Emissivity describes a material's ability to emit or release the thermal energy which it has absorbed. A perfect radiator (known as a "black body") will emit the entire amount of absorbed energy. A "real body" will always emit less energy than a "black body" at the same temperature. Emissivity (ε) is the ratio of radiation emitted of a given object or "real body" (Φ_r) and a "black body" (Φ_b) at the same temperature ($\varepsilon = \Phi_r / \Phi_b$). Thus, emissivity is a non dimensional quantity or factor between 0 and 1.

2. Methods

2.1. Overview

Temperature measurements were recorded on thermal features common in geothermal settings. We examined the temperatures of 40 thermal manifestations (Table 1) and grouped each feature into one of the following categories: (1) alkali chloride hot springs, (2) alkali chloride discharge channels, (3) acid sulphate pools, (4) mud pools, (5) steaming ground, and (6) fumaroles. We recorded the temperatures using: (i) an infrared camera, (ii) an infrared thermometer, and (iii) a digital temperature probe. For each feature we measured the temperature at the same site to enable a direct comparison of each technique. In the field emissivity values of 0.95 and 0.75 were used for the infrared measurements to assess the sensitivity of these techniques using different emissivity values. Following the field work back in the laboratory, the emissivity values were manipulated within the software package (SmartView 3.0) to obtain the best fit temperature for each feature. Figures 2-8 present matched visible light and infrared photographs of one feature representing each of the six categories. Tables 2-8 and figures 2-8 show the recorded data for each representative thermal feature. For our study, we assumed that the temperature recorded by the digital temperature probe is the most accurate so we assessed the infrared measurements in relation to the temperature probe readings. The six groups of thermal features in our study are separated into the two broad classifications of alkali chloride and acid sulphate features.

2.2 Techniques

Our digital temperature probe consists of a W500 K-type thermocouple cable with a measurement range from -50°C to >300°C with an accuracy of ± 0.3%. We used a 5 m long cable so our

measurements were limited by the length of the cable. The infrared thermometer is a compact hand-held thermometer with a dual laser targeting QM-7221 with sensitivity in the 8-14 µm wavelength. The thermometer has a range of -50°C to 650°C and a reading accuracy of ± 0.1%. A direct line of sight is required to measure the temperature. Our infrared camera is a Ti32 thermal imager, sensitive within the 8-14 µm wavelength. It is capable of measuring temperatures between -20°C and 600°C and is accurate to ± 2°C or 2 % whichever is greater at 25°C.

3. Results

3.1. Alkali Chloride Features

3.1.1. Alkali Chloride Hot Pools

We selected four alkali chloride hot pools for our study (Table 1). This feature type consists of clear, blue water as shown at Soda Fountain, Orakei Korako (Fig. 2A). At Soda Fountain, the water can be seen filling a pool that is well constrained by a rim of siliceous sinter. The pool is moderately steaming. The infrared image (Fig. 2B) detects the clearly defined hot water body and discharge channel, as well as the steam cloud ascending above the pool. For this feature the best fit emissivity value for the infrared camera was 0.71. At 0.71 emissivity value the infrared camera recorded a water temperature of 101.8°C which is very close to the measured temperature of 101.7°C (Table 2). In three of the four pools, the best fit emissivity value ranged between 0.71 and 0.78.

Feature Type	**Feature Name**	**Loc.**	**IR Thermometer (°C)**		**IR Camera (°C)**		**Best Ɛ / (°C)**	**T Probe (°C)**
			Ɛ = 0.95	***Ɛ = 0.75***	***Ɛ = 0.95***	***Ɛ = 0.75***		
Alkali Chloride Pools	Fred and Maggie's	3	97.8	100.8	95.0	99.6	0.78 / 99.0	99.0
	Soda Fountain	3	92.0	100.5	85.2	98.4	0.71 / 101.8	101.7
	Waiotapu Geyser	1	72.3	80.2	78.0	89.8	0.76 / 89.1	89.1
	Champagne Pool	1	67.9	79.2	72.5	83.4	0.89 / 75.4	75.4
Alkali Chloride Channels / Streams	Emerald Terrace	3	28.9	-	28.2	30.7	0.67 / 31.6	31.6
			41.8	42.0	42.7	48.1	0.90 / 43.8	43.9
			28.2	28.9	28.2	30.7	0.82 / 29.5	29.5
			31.9	33.2	31.4	34.4	0.86 / 32.6	32.6
	Sapphire Geyser	3	57.0	69.5	60.2	68.4	1 / 58.5	52.3
			36.5	36.9	32.5	35.8	0.67 / 37.5	37.6
			31.4	34.0	30.7	33.6	0.58 / 37.3	37.3
			27.0	27.1	25.8	27.4	0.65 / 28.6	28.5
Acid Sulfate Pools	Rainbow Crater	1	75.0	88.7	87.4	101.0	-	-
	Thunder Crater	1	84.6	90.5	84.6	97.7	-	-
	Opal Pool	1	37.1	40.0	35.7	39.7	0.60 / 44.1	44.0
	Frying Pan Flat	1	35.7	39.4	40.0	44.8	0.81 / 43.2	43.2
	Devil's Bath	1	22.5	20.7	25.3	23.6	-	-
	Te Kopia	2	39.6	42.2	41.3	46.6	0.84 / 43.9	43.8
Mud Pools	Devil's Ink Pots	1	59.3	66.9	64.3	73.2	-	-
			40.0	44.1	44.9	50.8	-	-
			24.0	44.7	32.4	35.6	-	-
			57.0	64.8	60.0	68.7	-	-
			32.4	34.3	40.7	45.6	-	-

			72.3	83.4	68.2	78.4	0.68 / 83.1	83.0
Steaming Ground	Devil's Ink Pot	1	43.4	46.3	48.1	54.6	-	~55.0-64.8
	Waiotapu Geyser	1	64.7	73.8	64.5	74.0	0.66 / 79.9	79.6
	Alum Cliffs	1	80.0 69.3	90.4 75.1	74.9 65.1	92.4 76.5	0.71 / 95.9 0.51 / 94.0	95.9 93.7
	Sulphur Cave	1	72.7 64.7	89.0 88.3	87.1 70.9	96.9 81.6	0.71 / 98.9 0.67 / 87.3	98.7 87.1
	Te Kopia	2	48.0 69.9	57.1 88.7	50.3 77.4	59.5 87.2	1 / 48.9 0.63 / 98.8	41.1 98.7
	Elephant Rock	3	65.1	71.8	77.1	88.8	0.80 / 85.4	85.4
Fumaroles	Elephant rock	3	66.4 51.0	91.8 55.7	91.6 52.7	107.5 60.1	0.91 / 94.8 1 / 51.3	95.0 51.1
	Kurapai Geyser area	3	92.5 84.0 73.5	107.5 93.2 88.9	85.3 80.7 83.6	98.6 89.6 89.1	0.74 / 99.4 0.73 /94.7 0.71 /99.9	99.1 95.1 99.9
	Rainbow Crater	1	84.8	109.3	97.2	112.4	0.93 / 98.7	98.8
	Te Kopia	2	70.9	80.3	76.0	87.6	0.70 / 91.4	91.4

Table 1. Specific features and temperature measurements recorded using infrared camera, infrared thermometer and digital temperature probe. Loc = sample location. IR = infrared. Best Ɛ/°C = emissivity value setting on the infrared camera for obtaining the closest temperature readings to the measured temperatures using the temperature probe / closest temperature.

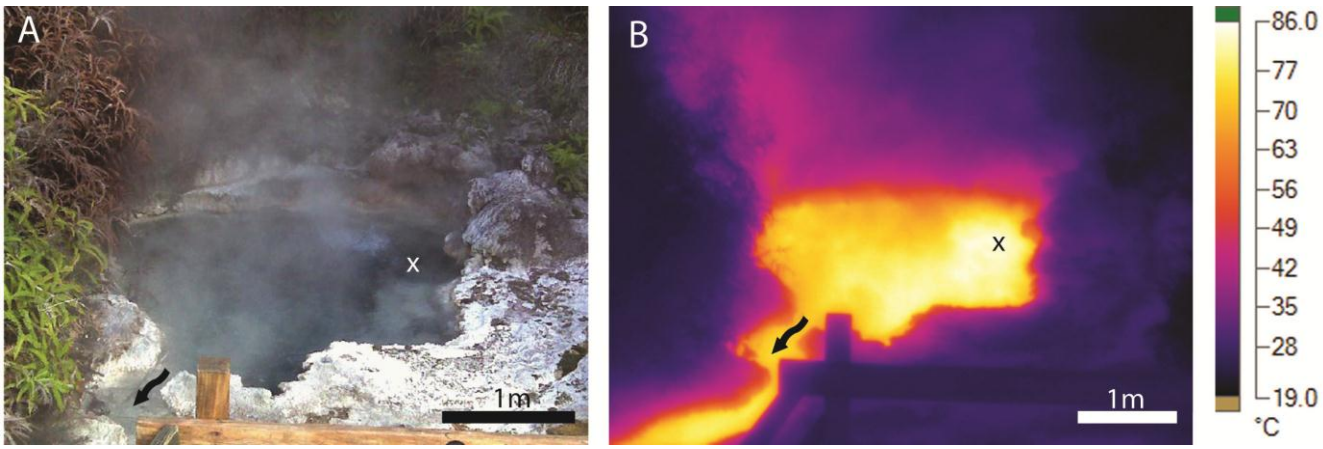

Fig. 2. Alkali chloride hot spring pool and discharge channel. Soda Fountain, Orakei Korako. X = site of temperature measurements. Arrows indicate discharge channel. (A) Visible light photograph shows clear, blue, alkali chloride water with well-defined discharge channel. (B) Infrared image captures the areas of increased heat in this alkali chloride feature, including zones of high temperature up-flow (white areas) within the pool and the increased temperature from the steam ascending above the pool.

The best fit emissivity value for the Champagne Pool at Waiotapu was 0.89, a considerably higher emissivity value than the other alkali chloride pools. Unlike the other features analysed in this group, large clouds of steam were continually discharging from the surface of the Champagne Pool. This could be responsible for the need of a higher emissivity value when using the infrared camera. The hand-held infrared thermometer is less sensitive to the steam as it has a focussed, concentrated beam of infrared light that you can point directly at the pool surface, as opposed to the broad overview captured

by the infrared camera. These examples show the effect of discharging steam on the emissivity values. For alkali chloride pools with no steam an emissivity value of 0.71 to 0.78 was required while the emissivity value needed to be increased to 0.89 for pools discharging abundant steam.

Temperatures measured in the field of individual spots using the infrared camera and infrared thermometer where the emissivity value was 0.75 generally varied by up to 4°C, while they varied by up to 7 °C when the emissivity value was 0.95 (Table 1).

Infrared Thermometer (°C)		**Infrared Camera (°C)**		**Best fit *Ɛ to Infrared camera measurements /°C**	**Temperature Probe (°C)**
***Ɛ = 0.95**	***Ɛ = 0.75**	***Ɛ = 0.95**	***Ɛ = 0.75**		
92.0	100.5	85.2	98.4	0.71 / 101.8	101.7

*Table 2. Temperature measurements recorded at site X in Figure 2. *Ɛ = emissivity value.*

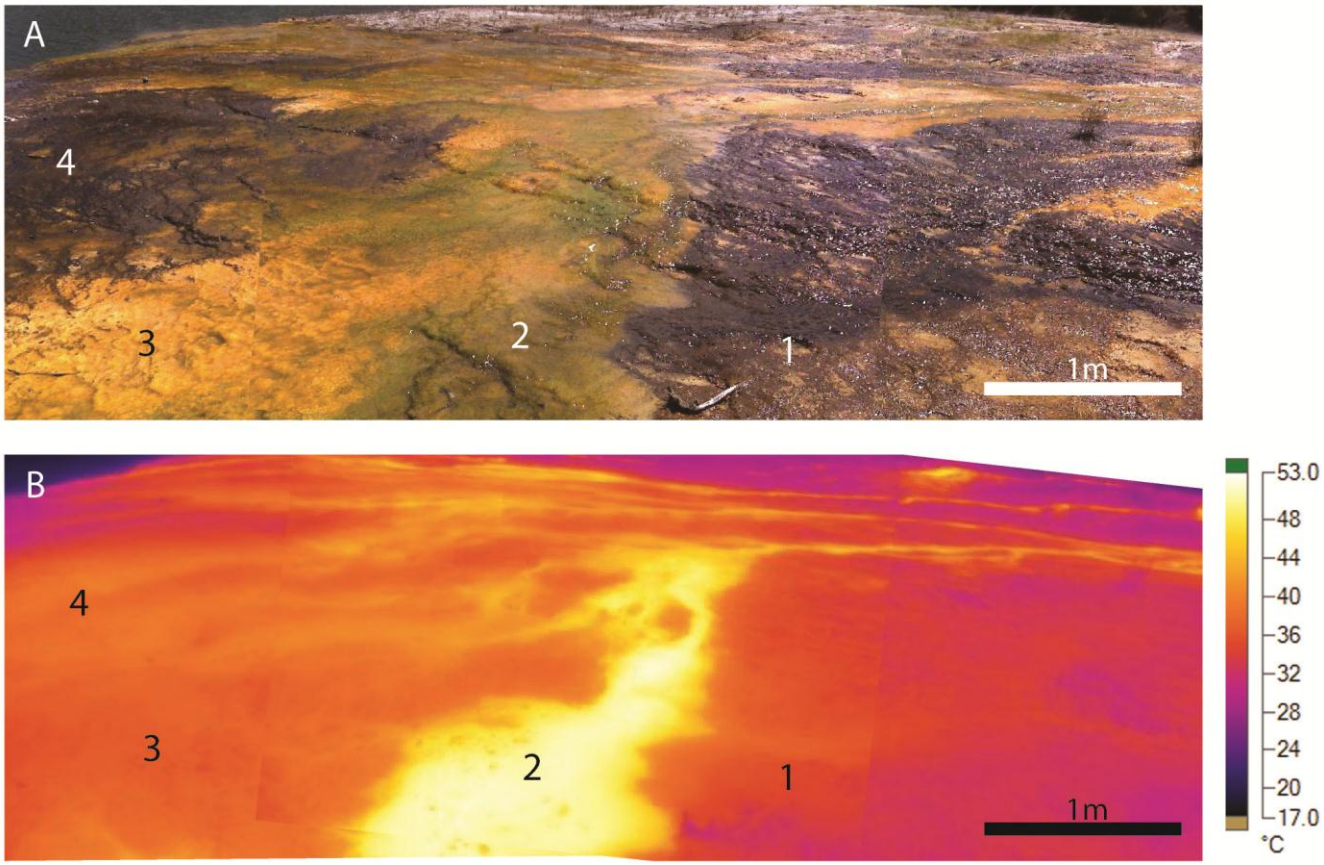

Figure 3. Discharge channels from alkali chloride hot springs flowing over sinter terrace referred to as the Emerald Terrace located at Orakei Korako. Temperature measurements taken at sites 1, 2, 3 and 4. (A) Visible light photograph shows mid-temperature (35-59 °C) microbial mats in orange and low-temperature (<35 °C) microbial mats in black thriving in the thermal water. (B) Infrared image captures temperature distribution of thermal water over Emerald Terrace. Temperatures shown reveal similar temperature gradients to those indicated by microbial communities.

3.1.2. Alkali Chloride Discharge Channels

Four sites on Emerald Terrace and four sites within the Sapphire Geyser discharge channel area, both located at Orakei Korako were selected for measuring the water temperature of sheet flow of alkali chloride fluid over expansive sinter terraces (Table 1). Living in these environments are coloured microbial mats (Fig. 3A). A temperature gradient profile is shown by the distribution of the coloured microbial mats where the orange mats live in water with a temperature between 35 and 59°C and the black mats live where the temperature is < 35°C. Our digital thermometer readings confirm that the coloured mats on Emerald Terrace are associated with these specific temperature ranges. One exception is site 3 (Fig. 3A) which is covered in orange mats and should have a temperature between 35-59°C. However, here the measured temperature is only 29.5°C. This lower than expected temperature is due to minimal water flowing over these mats and the mats are drying out. The infrared image of Emerald Terrace (Fig. 3B) shows the flow pathways of the discharge area and distinguishes mid- from low-temperature flow channels. Changing the infrared camera emissivity values to get the best fit to the measured temperature profile shown in Figure 3 recorded a range of emissivity values between 0.67 and 0.9 (Table 3).

	Infrared thermometer (°C)		**Infrared Camera (°C)**		**Best fit *Ɛ to Infrared camera measurements / °C**	**Temperature Probe (°C)**
	***Ɛ = 0.95**	***Ɛ = 0.75**	***Ɛ = 0.95**	***Ɛ = 0.75**		
1	28.9	-	28.2	30.7	0.67 / 31.6	31.6
2	41.8	42.0	42.7	48.1	0.90 / 43.8	43.9
3	28.2	28.9	28.2	30.7	0.82 / 29.5	29.5
4	31.9	33.2	31.4	34.4	0.86 /32.6	32.6

*Table 3. Temperature measurements recorded at sites 1, 2, 3 and 4 shown in Figure 3. *Ɛ = emissivity value.*

The best fit emissivity values for temperature measurements taken in Sapphire Geyser discharge channel ranged between 1.0 and 0.58. Temperatures recorded at identical spots in the field using an emissivity value of 0.75 on the infrared camera and infrared thermometer revealed almost identical temperatures. This was also shown when we set the emissivity value to 0.95 (Table 1).

3.2. Acid Features

3.2.1. Acid Sulphate Pools

Six opaque, acid sulphate pools were measured for this study (Table 1). Many of these features consist of acid sulphate water in the base of > 5 m deep depressions. Unfortunately we could not reach the water to measure the temperature with our probe in three pools as we were restricted by the length of our 5 m cable. Where we could not access the feature, the infrared temperature readings from both the camera and thermometer showed a range of values. Some measurements correlated well while others showed a poor correlation. One explanation for the poor correlation could be that distance from the feature made it difficult to isolate a single site within the feature. To be able to directly compare readings using different temperature measuring methods it is essential that the same site is measured by all devices.

For our study when the infrared camera and infrared thermometer were set with an emissivity value of 0.75 the temperatures were within ± 5°C of the measured temperature in the three pools we were able to measure with the temperature probe. When we changed the emissivity value to 0.95 the temperatures were ± 8°C of the measured temperature. When the emissivity values were set on the infrared camera

to get a best fit to the measured temperatures, a range of emissivity values between 0.60 and 0.84 was required (Table 1).

The Opal Pool at Waiotapu (Fig. 4A) demonstrates the characteristic opaque nature of acid sulphate water. This water type differs from the alkali chloride water in that it is translucent, opaque or murky. The infrared image of the Opal Pool (Fig. 4B) detects not only the warm water within the pool but also areas with increased temperature surrounding the pool. Some of the highest temperature sites are located not in the pool itself but in the overflow areas. These high temperature locations indicate sites where there is increased steam ascending from the subsurface. Without infrared imaging, it would not be possible to record this process. The temperature was measured at one site within Opal Pool using the temperature probe (T = 44°C). The best fit emissivity value set in the infrared camera to obtain a temperature close to 44 °C was 0.60 (Table 4).

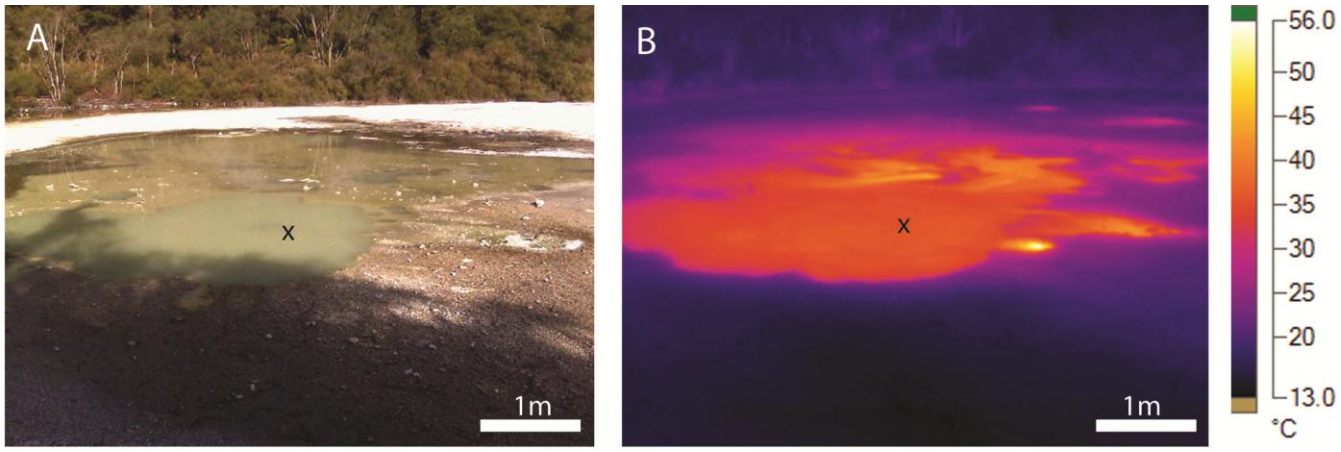

Fig. 4. Typical opaque, acid sulphate pool. Opal Pool, Waiotapu. X = site of temperature measurements. (A) Visible light photograph shows the opaque green water of this acid sulphate pool. On one side of the pool, a thin sheet of water is present where the pool is overflowing. (B) Infrared image clearly defines the pool and its overflow areas as sites of higher temperature.

Infrared Thermometer (°C)		**Infrared Camera (°C)**		**Best fit *Ɛ to Infrared camera measurements /°C**	**Temperature Probe (°C)**
***Ɛ = 0.95**	***Ɛ = 0.75**	***Ɛ = 0.95**	***Ɛ = 0.75**		
37.1	40.0	35.7	39.7	0.60 / 44.1	44.0

*Table 4. Temperature measurements recorded at site X in Figure 4. *Ɛ = emissivity value.*

3.2.2. Mud Pools

Six temperature measurements within different mud pools at Waiotapu were chosen for this study (Table 1). The mud in these pools was mixed with a considerable amount of rain water giving them the appearance of brown, opaque, liquid mud pools (Fig. 5A). A temperature of 83.0°C was recorded using the temperature probe at one site within this pool. With the infrared camera and the thermometer emissivity values set at 0.75, temperatures of 78.4°C and 83.4°C were recorded. When the emissivity value was set at 0.95 the camera measured a temperature of 68.2°C and the thermometer measured 72.3°C. Manipulating the emissivity value to get the best fit to the measured temperature revealed that an emissivity value of 0.68 produced the best correlation (Table 5).

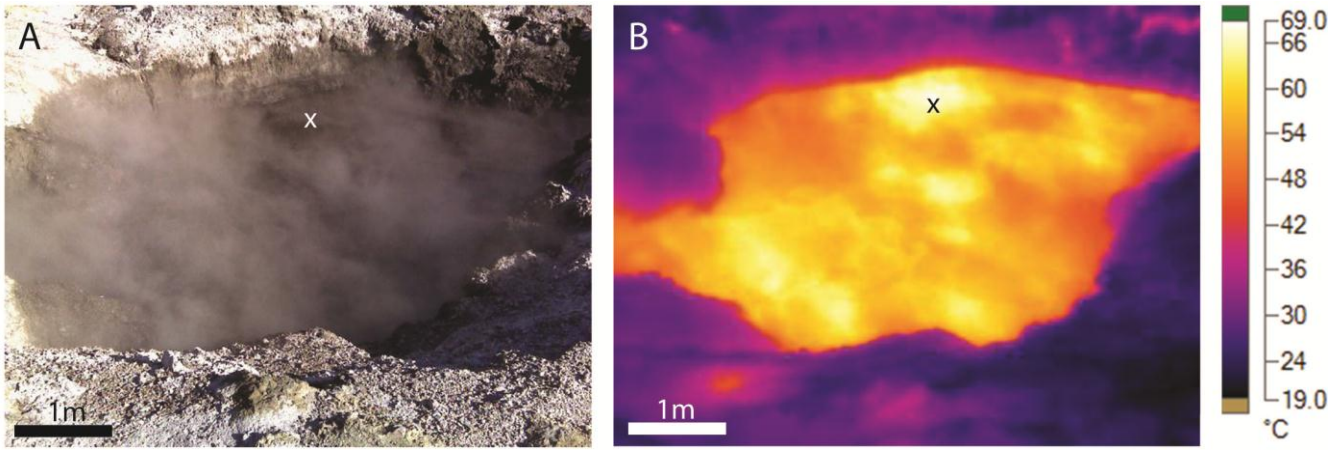

Figure 5. Brown, opaque, bubbling and steaming mud pool at Devil's Ink Pot, Waiotapu. X = site of temperature measurements. (A) Visible light photograph. (B) Infrared photograph.

The temperatures of five other mud pools were recorded using only the two infrared methods. Four of the five mud pool sites recorded a slightly higher temperature with the infrared camera. The infrared image of the Devil's Ink Pots revealed multiple hot up-flow zones within the pool (Fig. 5B), not obvious in the visible light photograph (Fig. 5A). Our higher temperature values recorded by the infrared camera could be explained by the distribution of hot up-flow zones. As they are not obvious without the infrared camera, the hand-held infrared thermometer may be recording temperatures only millimetres away from the camera measurement site, which would result in slightly lower temperature recordings.

Infrared Thermometer (°C)		**Infrared Camera (°C)**		**Best fit *Ɛ to Infrared camera measurements /°C**	**Temperature Probe (°C)**
***Ɛ = 0.95**	***Ɛ = 0.75**	***Ɛ = 0.95**	***Ɛ = 0.75**		
72.3	83.4	68.2	78.4	0.68 / 83.1	83.0

*Table 5. Temperature measurements recorded at site X in Figure 5. *Ɛ = emissivity value.*

3.3.3. Steaming Ground

Nine sites of steaming ground from Waiotapu, Te Kopia and Orakei Korako were examined in this study. For this category the temperatures measured using the digital temperature probe varied between 40 and 99°C. In most cases, measurements taken by using the emissivity value of 0.75 recorded temperatures closer to the measured temperature (±5 to 20°C). Measurements taken using an emissivity value of 0.95 were consistently lower than those measured using the 0.75 emissivity value and the digital temperature probe (±10 to 30°C). The best fit emissivity values for these features varied between 0.51 and 1. The variable and diffuse nature of steam that discharged from these features may be contributing to the range of temperature values recorded for this feature type as it was difficult to measure the same spot with all three temperature techniques at exactly the same time.

Steaming ground at Elephant Rock, Orakei Korako (Fig. 6A) is a typical example of the steaming ground environment commonly found in geothermal settings. It consists of irregular and diffuse discharge of steam and gases resulting in a patchy distribution of clay alteration that has occurred via

acidic steam condensate overprinting. While this ground is usually hot to the touch, often steam is not present giving the impression the surface is cool. Here, infrared imagery is very useful as it quickly and easily maps all the sites of elevated temperature (Fig. 6B). This type of ground is the most dangerous ground to walk over as the hydrothermal alteration process often weakens the ground making it unstable. For the steaming ground at Elephant Rock the best fit emissivity value was 0.8 (Table 6).

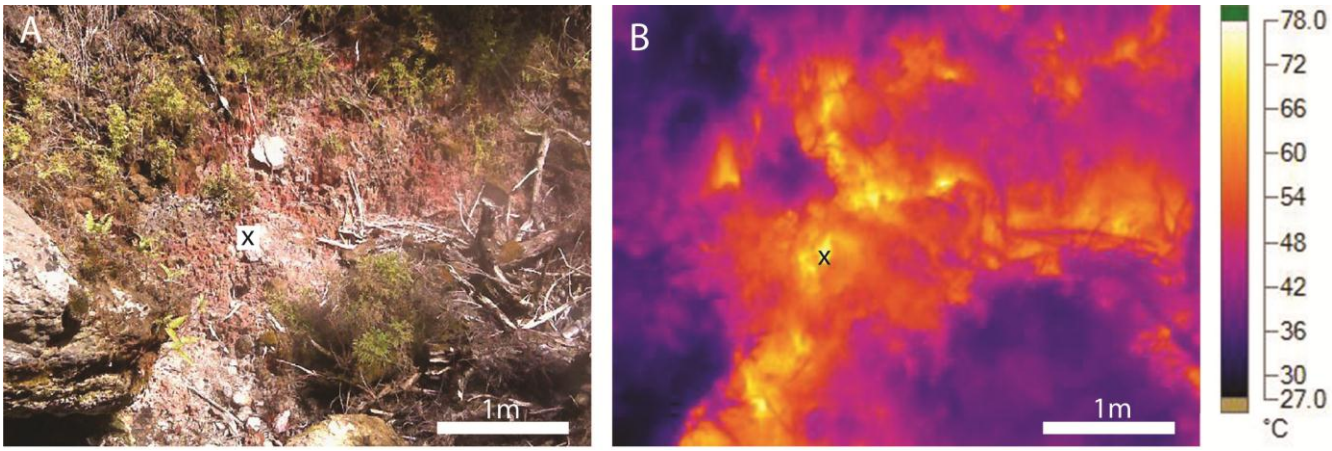

Fig. 6. Photographs of steaming ground at Elephant Rock, Orakei Korako. X = site of temperature measurements. (A) Visible light photograph showing hydrothermal alteration of the ignimbrite to clay (red and white areas) and thermally stressed vegetation. (B) Infrared photograph reveals the patchy distribution of heat discharging from the area.

Infrared Thermometer (°C)		Infrared Camera (°C)		Best fit *Ɛ to Infrared camera measurements /°C	Temperature Probe (°C)
*Ɛ = 0.95	*Ɛ = 0.75	*Ɛ = 0.95	*Ɛ = 0.75		
65.1	71.8	77.1	88.8	0.80 /85.4	85.4

*Table 6. Temperature measurements recorded at site X in Figure 6. *Ɛ = emissivity value.*

Figure 7 illustrates another example where < 10 mm diameter steam vents are easily visible using the infrared camera but are not obvious in the visible light photograph. Unintentionally walking on these tiny vents could produce a significant burn. Infrared imagery assists in detecting sites of high heat flow and identifies sites that may be unstable and dangerous to walk on. The best fit emissivity value for this site was 0.67 (Table 7), considerably lower than 0.8 emissivity values regarded at Elephant Rock (Table 6).

Infrared Thermometer (°C)		Infrared Camera (°C)		Best fit *Ɛ to Infrared camera measurements /°C	Temperature Probe (°C)
*Ɛ = 0.95	*Ɛ = 0.75	*Ɛ = 0.95	*Ɛ = 0.75		
64.7	88.3	70.9	81.6	0.67 / 87.3	87.1

*Table 7. Temperature measurements recorded at site X in Figure 7. *Ɛ = emissivity value.*

3.3.4. Fumaroles

Seven fumaroles from Orakei Korako, Waiotapu and Te Kopia were chosen for the fumarole section of this study (Table 1). When the emissivity values for both infrared techniques were set at 0.75 the temperatures were generally ±10°C of the measured temperature, while when the emissivity value was

set at 0.95 this increased to ±20°C. The intermittent pulsing of fumaroles makes it difficult to assess the temperature at exactly the same time using all three techniques and this may account for the variability recorded within these features. The emissivity values that produce the best fit to measured temperatures range from 0.70 to 1.

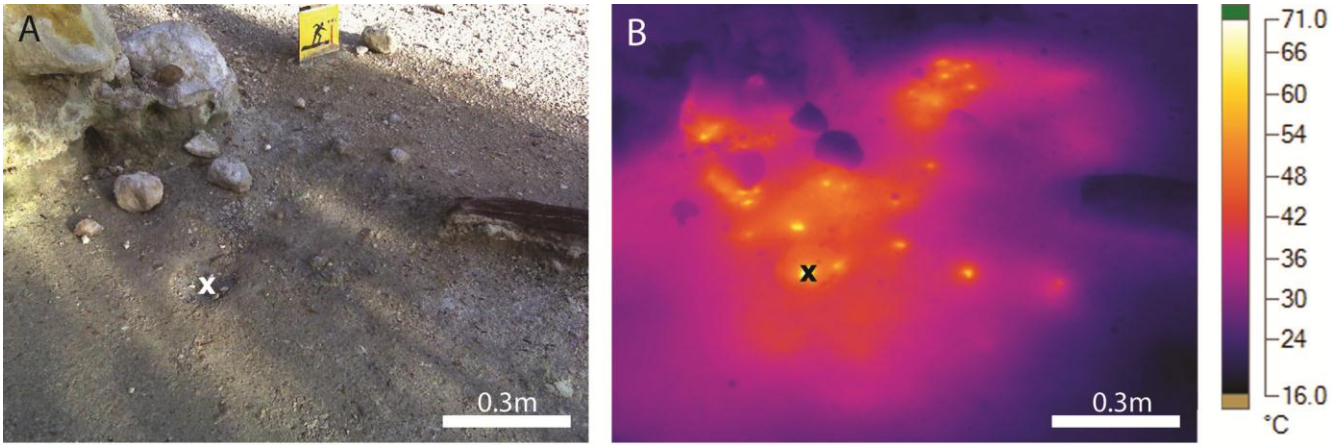

Figure 7. *Small, well-defined vents in area of warm ground. X = site of temperature measurements. (A) No evidence of hot spots shown in visible light photograph. (B) Infrared image clearly defines sites of high temperature not visible in (A)*

Figure 8A illustrates the nature of a typical fumarole from a geothermal setting. Fumaroles discharge a high velocity of steam and gas and the vents are often surrounded by sulphur crystals. Infrared imaging of these features shows the distribution of high temperatures that occur not only in the vent, but also in the surrounding area (Fig. 8B). One site within a fumarolic vent at Waiotapu (Fig. 8) showed a measured temperature of 98.8°C (Table 8). The best fit emissivity value for this site was 0.93.

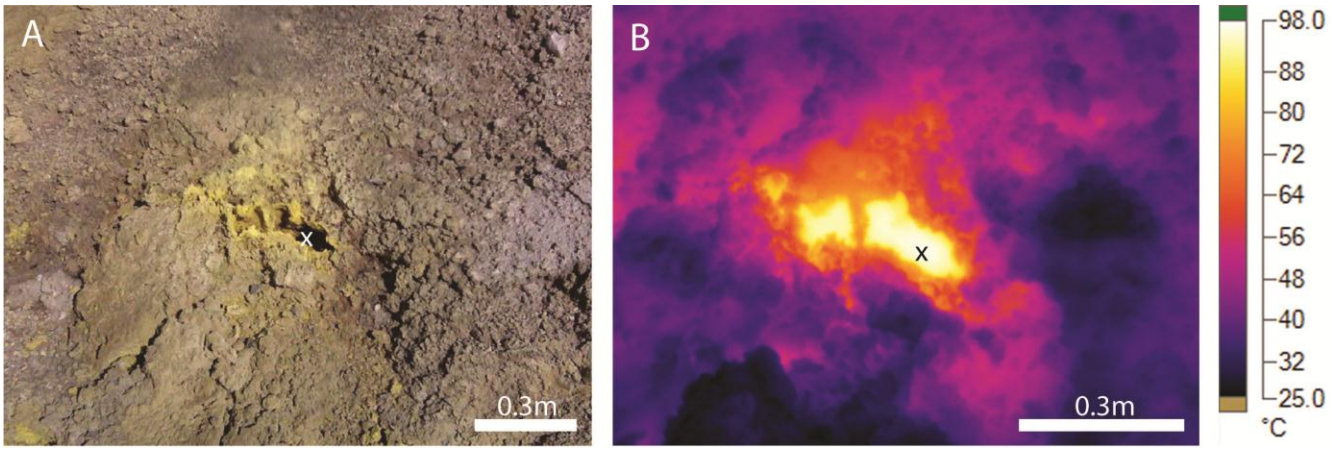

Fig. 8. Photographs of a fumarolic vent at Waiotapu. X = site of temperature measurements. (A) Visible light photograph of a fumarole with yellow sulphur crystals on area surrounding vent. (B) Infrared image clearly detects the high temperature within the vent and provides a thermal gradient profile of the surrounding area.

4. Conclusions

Understanding the heat flow from the surface above a geothermal system is an important component of geothermal exploration. Evaluation of the surface heat flow includes measuring the ground temperature

which can be achieved using infrared imaging. Aerial infrared imaging is useful but expensive. Our study shows that images taken using a hand-held infrared camera are ideal for mapping the surface thermal profile of any given area.

Infrared Thermometer (°C)		**Infrared Camera (°C)**		**Best fit *Ɛ to Infrared camera measurements /°C**	**Temperature Probe (°C)**
***Ɛ = 0.95**	***Ɛ = 0.75**	***Ɛ = 0.95**	***Ɛ = 0.75**		
84.8	109.3	97.2	112.4	0.93 / 98.7	98.8

*Table 8. Temperature measurements recorded at site X in Figure 8. *Ɛ = emissivity value.*

Infrared imaging using a hand-held camera can be used for all types of thermal features. However to obtain accurate temperature measurements, a range of emissivity values are required for the different feature types. Therefore it is appropriate to use a range of emissivity values to record a measured temperature at the time the infrared image is taken. We found that for all thermal manifestations, infrared temperature measurements using both the infrared camera and infrared thermometer were usually lower than those recorded using the digital thermometer. This is due to the differences in the three techniques. The infrared methods detected the temperature on the surface of a feature that consists of a combination of solar radiation heat and heat flow from the thermal feature. The digital thermometer recorded the kinetic temperature below the surface of the water and inside vents.

It is more difficult to obtain accurate temperature readings from steaming features. When there is an abundance of steam discharging from a feature, the camera focused on the steam rather than the vent often resulting in a lower temperature reading. The steam prevented a clear line of sight to the surface of the hot pool or mouth of the steam vent or fumarole. However, when the steam was not too abundant the infrared thermometer could penetrate the steam with its narrow focussed beam. Discharging steam often pulses from these features and the temperature within the steam at any given time can be highly variable. Despite these difficulties we were able to obtain useful temperature data from all steaming features.

Our infrared images captured all sites of elevated temperature, many of which are not obvious in the visible light photography or to the naked eye. From the thermal imaging it is possible to identify if there is any preferred orientation (e.g., East-West or North -South) or clustering of areas with high heat flow. Location and orientation of surface features that discharge heat provide information that can be related to the regional geologic and structural trends. This information is also important when developing a local hydrologic, geologic, geochemical or geophysical model of an area. Infrared maps are useful when working in geothermal environments as they identify cool versus hot areas making field work less dangerous. Many sites within a geothermal area are inaccessible due to unstable ground or steep terrain. The use of an infrared camera enables a greater number of thermal features to be mapped as surface heat can be detected and imaged from a distance.

Acknowledgements

We would like to thank The Royal Society of New Zealand, Strategic Relocation Fund and the Foundation for Research Science and Technology, Geothermal Research Grant held at the University of Auckland for supporting this work. Special thanks to Cheng Yii Sim, Madison Frank and Gary Smith for assistance with field work.

References

Ball M., and H. Pinkerton, 2006. Factors affecting the accuracy of thermal imaging cameras in volcanology. *Journal of Geophysical Research*, **111**, pp. 1-14.

Coolbaugh M.F., C. Kratt, A. Fallacaro, W.M. Calvin, and J.V. Taranik, 2006. Detection of geothermal anomalies using Advanced Spaceborne Thermal Emission and Reflection Radiometer (ASTER) thermal infrared images at Bradys Hot Springs, Nevada, USA. *Remote Sensing of Environment*, **106**, pp. 350-359.

Dickinson D.J., 1975. Airborne infra-red survey of the Tauhara geothermal field, New Zealand. *Proceedings of the Second United Nations Symposium on the Development and Use of Geothermal Resources*, v. 2, pp. 955-961.

Oppenheimer C., P. Bani, J.A. Calkins, M.R. Burton, and G.M. Sawyer, 2006. Rapid FTIR sensing of volcanic gases released by Strombolian explosions at Yasur volcano, Vanuatu. *Applied Physics Bull.*, v. 85, pp. 453-460.

Qiming Q., Z. Ning, N. Peng, and C. Leilei, 2011. Geothermal area detection using Landsat ETM+ thermal infrared data and its mechanistic analysis - A case study in Tengchong, China. *International Journal of Applied Earth Observation and Geoinformation*, v. 13, pp. 552-559.

Stevenson J., and N. Varley, 2008. Fumarole monitoring with a handheld infrared camera: Volcán de Colima, Mexico, 2006-2007. *Journal of Volcanology and Geothermal Research*, v. 177, pp. 911-924.

Yuhara K., M. Sekioka, and S. Ehara, 1978. Infrared Measurement on Satsuma-iwojima Island, Kagoshima, Japan, by Helicopter-Borne Thermocamera. *Archiv fur meteorologie geophysik und bioklimatologie*, Series A, v. 27, pp. 171-181.